ACS Infectious Diseases

Article

Cite This: ACS Infect. Dis. 2018, 4, 926−935

pubs.acs.org/journal/aidcbc

Carbapenems and Lipid Bilayers: Localization, Partitioning, and Energetics

Adree Khondker, Dylan J. Malenfant, Alexander K. Dhaliwal, and Maikel C. Rheinstädter*

Department of Physics and Astronomy, McMaster University, 1280 Main Street West, Hamilton, Ontario L8S 4M1, Canada
Origins Institute, McMaster University, Hamilton, Ontario L8S 4M1, Canada

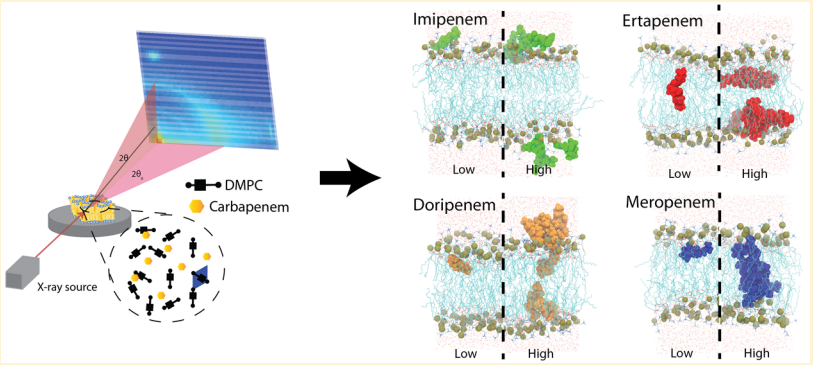

ABSTRACT: Carbapenems are broad-spectrum antibiotics used today to treat otherwise antibiotic resistant bacteria. As their target transpeptidase is located within the periplasm of the Gram-negative bacteria, they can participate in nonspecific interactions between the inner leaflet of the outer membrane and the outer leaflet of the inner membrane. We, therefore, studied the interaction of the four most clinically relevant carbapenems, namely, imipenem, doripenem, ertapenem, and meropenem, with model phospholipid bilayers made of 1,2-dimyristoyl-*sn*-glycero-3-phosphocholine (DMPC) using molecular dynamics (MD) simulations and X-ray diffraction at low and high concentration of the drugs corresponding to 1 and 8 mol % (with respect to the number of membrane lipids). Membrane solubility was found to decrease from imipenem to doripenem, ertapenem, and finally meropenem. At low concentrations, membrane insertion was found to be a two step process, where the drugs first adsorb to the lipid head groups before inserting through a rotation of the molecule. At higher drug concentrations, the molecules were found to form aggregates in the aqueous phase before making contact with the membranes and spontaneously inserting into the bilayers. Two populations of imipenem were found: in the headgroup at ∼17 Å from the bilayer center and an inserted population at *z*-values of about 7 Å. Other carbapenems were found to localize in the tail groups with meropenem at ∼10 Å, doripenem at ∼8 Å, and ertapenem at ∼8 Å. The observed membrane solubility of carbapenems can potentially impact the availability of the drug to the target penicillin-binding proteins, potentially affecting their clinical efficacy.

KEYWORDS: *carbapenems, imipenem, doripenem, ertapenem, meropenem, antibiotics, drug−membrane interaction, membrane solubility*

Downloaded via MCMASTER UNIV on January 7, 2019 at 13:56:48 (UTC).
See https://pubs.acs.org/sharingguidelines for options on how to legitimately share published articles.

With the arrival of increased antibiotic resistant bacteria,[1] novel derivatives and clinical isolates of the broader pencillin-like class of antibiotics have been effective in the treatment of superbugs.[2] Carbapenems are broad-spectrum β-lactam antibiotics, which inhibit transpeptidases reponsible for cell wall synthesis within the bacterial membrane complex.[3] The four most clinically relevant carbapenems are imipenem, doripenem, ertapenem, and meropenem.[4] The molecular structure of the drugs is depicted in Figure 1. Although carbapenems act specifically upon transpeptidases,[5] they undergo a variety of nonspecific interactions with components of Gram-negative bacterial membranes, such as transport to and through the periplasm, potentially affecting the clinical availability to transpeptidase.[6−8] However, many of the mechanisms involving the interactions of carbapenems in the specific membrane environment remain understudied.

The current model of action for carbapenems suggests that the core lactam is solely responsible for the inhibition of cell-wall synthesizing transpeptidases.[3] Literature suggests that carbapenems enter the periplasm by active uptake through ion and amino acid transporters.[9] Membrane interactions and potential membrane absorption of carbapenems may, thus, impact their availability in the transmembrane space, as sketched in Figure 2.

Phospholipids are a major component of the bacterial inner membrane and the inner leaflet of the bacterial outer membrane in Gram-negative bacteria.[10] The presence of organized phospholipids creates a hydrophilic−hydrophobic interface, which can modulate the behavior and effects of many

Received: September 19, 2017
Published: March 27, 2018

© 2018 American Chemical Society

DOI: 10.1021/acsinfecdis.7b00156
ACS Infect. Dis. 2018, 4, 926−935

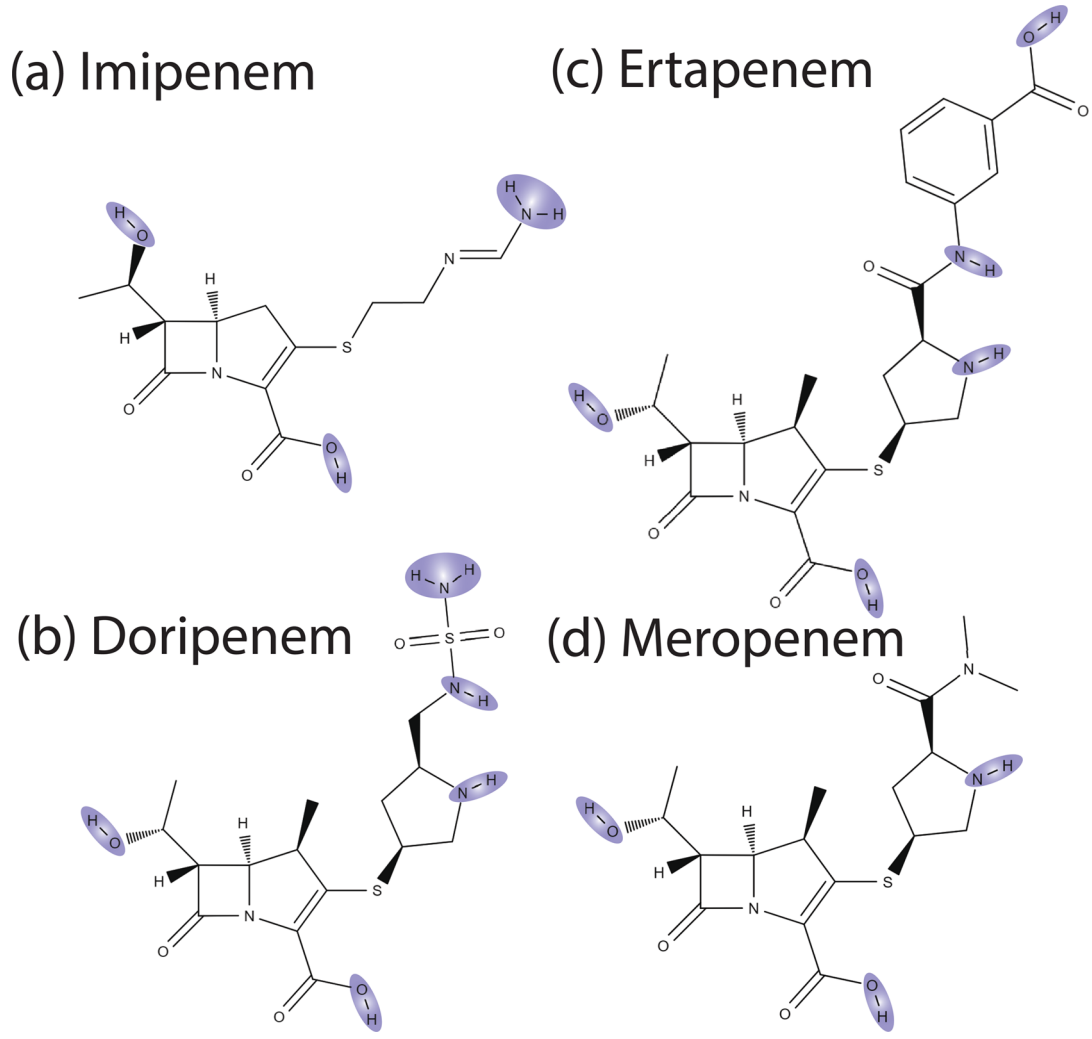

Figure 1. Schematic of the four most clinically relevant carbapenems: imipenem, doripenem, ertapenem, and meropenem. Carbapenems consist of a nonpolar aromatic β-lactam, while the additional functional groups can give rise to an overall polarity of the molecule. Potential hydrogen bond donors are highlighted in blue.

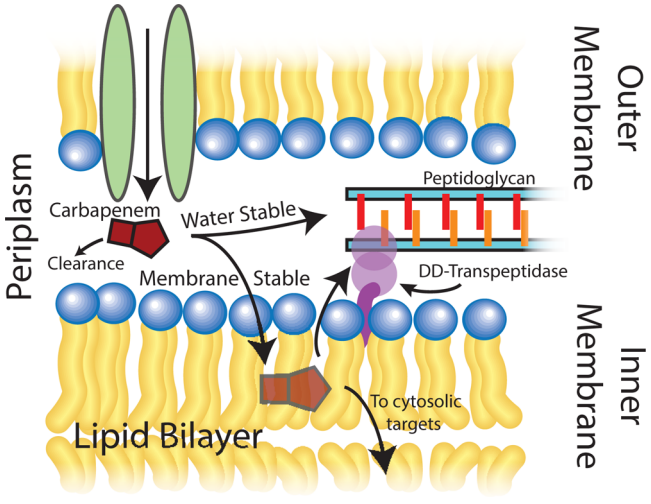

Figure 2. Carbapenems are broad-spectrum antibiotics, which target transpeptidase mainly located within the periplasm of the Gram-negative bacteria. Carbapenems are transported into the periplasm actively. Potential partitioning of the carbapenems into lipid bilayers may influence their availability toward inhibiting transpeptidases.

bioactive molecules. Previous molecular dynamics (MD) simulations focused on characterizing the interactions of carbapenems with transpeptidases or β-lactamases.[11,12] Interactions of carbapenems with the lipid bilayer have been limited due to the inert role they seem to play in carbapenem action. Recent findings with other membrane-independent antibiotics have shown that the former title may no longer be accurate. For example, kanamycin, a bacterial DNA replication inhibitor, was recently found to disorder the membrane,[13] indicating that the cell membrane may play an important role in understanding and modeling also the functioning of carbapenems.

We conducted MD simulations and X-ray diffraction experiments of imipenem, doripenem, ertapenem, and meropenem in contact with 1,2-dimyristoyl-*sn*-glycero-3-phosphocholine (DMPC) lipid bilayers at low and high carbapenem concentrations of ∼1 mol % and 8 mol %, respectively (drug concentrations are given with respect to the number of lipid molecules). Position, partitioning, and insertion kinetics of the molecules were determined from simulations and experiments, and the interaction with the membrane and impact on membrane properties were studied. We found that the carbapenems have very different membrane affinities with

DOI: 10.1021/acsinfecdis.7b00156
ACS Infect. Dis. 2018, 4, 926−935

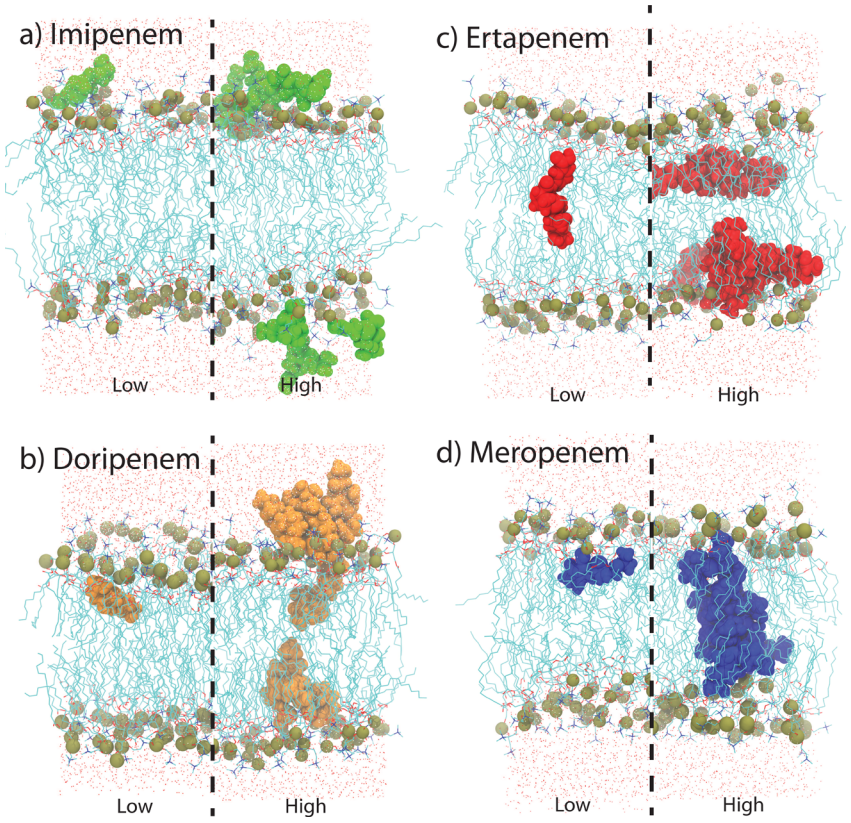

Figure 3. Snapshots of imipenem (a), doripenem (b), ertapenem (c), and meropenem (d) after 200 ns of simulation at low (~1 mol %) and high drug concentrations (~8 mol %). Doripenem, meropenem and ertapenem were found to spontaneously insert into the bilayers at low and high drug concentrations while imipenem showed no membrane solubility even after 400 ns of simulations.

imipenem, doripenem, ertapenem, and meropenem in increasing order.

RESULTS

Carbapenems are applied to many types of infections, from the respiratory tract to polymicrobic infection. For this reason, it is difficult to derive an exact molar carbapenem concentration. In order to estimate a typical dosage, we assumed two conditions: a single carbapenem molecule in a 128 lipid bilayer patch, mimicking a low concentration of ~1 mol %, or ten carbapenem molecules to account for drug−drug interactions at elevated concentrations of ~8 mol %. By assuming the volume of a bacterium to be 0.7 μm^3 or 7×10^{-13} mL, we can multiply this by a typical carbapenem blood concentration (minimum inhibitory concentration, MIC) of 0.125 μg/mL.[14] Dividing by, for instance, imipenem's molar mass of 300 g/mol and multiplying by Avogadro's constant, we find that, at MIC concentrations, there are 175 imipenem molecules per bacterial cell.[15] The number of bacterial lipids was reported to be 5.4×10^5;[16] therefore, dividing the number of carbapenems per cell to lipids per cell, we find the MIC to be 3.2×10^{-2} mol %. Our experiments and simulations at 1 and 8 mol %, thus, correspond to highly elevated drug concentrations.

Simulations were composed of 128 DMPC lipids at a hydration of 30 water molecules per lipid and 15 Na^+ and Cl^- ions, resulting in ~18 000 atoms. The GROMOS 54a7 forcefield, modified with Berger lipid parameters, was used with the GROMACS 5.1.4 MD package. The systems were prepared with the same parameters as in ref 17. The specific methods used in the analysis are given in the Methods section. Snapshots of the different simulation sequences for low and high drug concentrations are shown in Figure 3.

Carbapenems consist of a nonpolar aromatic core, while the additional functional groups can give rise to an overall polarity of the molecule. In the simulations, the drug molecules were added to the aqueous layers. As a first finding, doripenem, meropenem, and ertapenem spontaneously partitioned into the membranes within 50 ns of simulation, while imipenem made contact with the lipid head groups without inserting into the membranes, even after 400 ns of simulations. At low concentrations, the larger carbapanems (doripenem, meropenem, and ertapenem) undergo a two step insertion sequence: they first adsorb to the bilayer and then rotate upon insertion.

The individual insertion kinetics is shown in Figure 4. By analyzing individual simulation frames, the position of the molecules as a function of time can be calculated for the different functional groups. In simulations with a single molecule of these drugs with a lipid bilayer, the hydrophilic end of the molecule attracts and intercalates with the head groups; this is the adsorption step. The molecule then rotates along the bilayer normal, inserting into the bilayer while maintaining the favorable interaction with a committed angle. Finally, the drug penetrates further into the acyl tails while maintaining this angle. Imipenem did not insert into the bilayer with high stability over 400 ns of simulation and was found to stay intercalated with the lipid head groups. The corresponding relative insertion velocity (shown in Figure 4e) was found to increase from imipenem to doripenem, ertapenem, and meropenem.

DOI: 10.1021/acsinfecdis.7b00156
ACS Infect. Dis. 2018, 4, 926−935

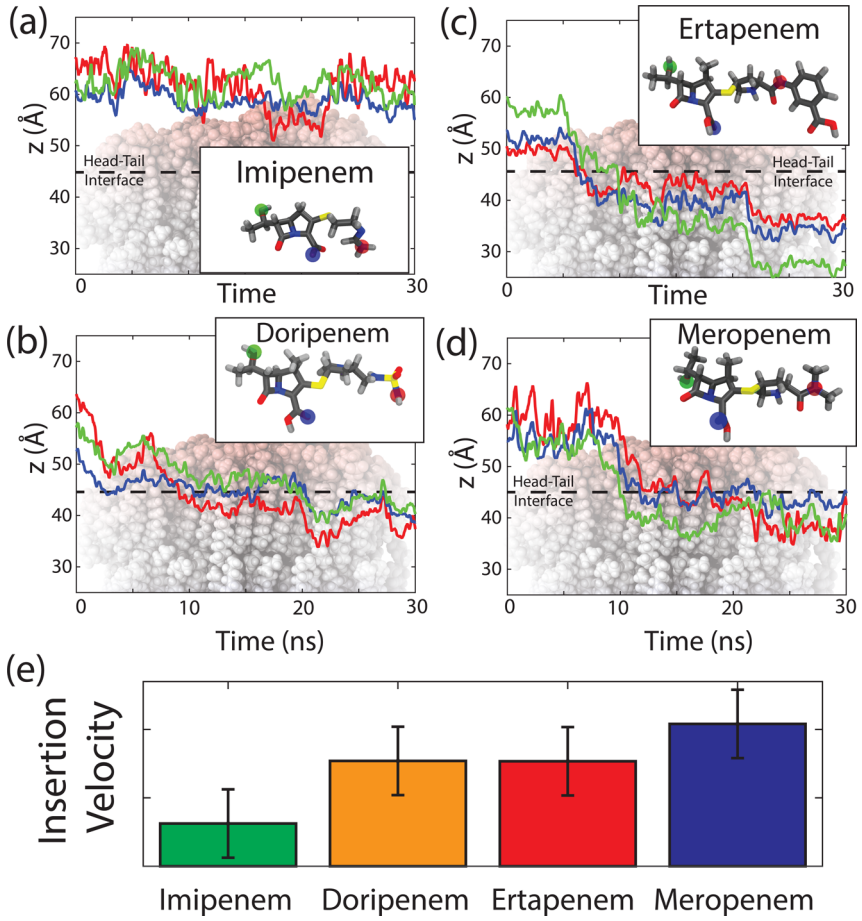

Figure 4. Insertion kinetics of individual molecules of carbpanems (a) imipenem, (b) doripenem, (c) ertapenem, and (d) meropenem. Line colors represent different functional groups and correspond to the colored atoms in each antibiotics molecule shown. Insertion is shown over 30 ns. (e) While imipenem did not insert into the bilayers within the time of the simulations (400 ns), doripenem, ertapenem, and meropenem were found to insert spontaneously, in ascending order of insertion velocity (as calculated from slope of the center-of-mass motion of the drug).

At high concentrations, an additional aggregation step prefaces this insertion and synergistically promotes the insertion of the carbapenems into the bilayer. Snapshots of the insertion kinetics at high concentrations of the drug molecules is shown in Figure 5. The drugs were found to aggregate on the surface of the bilayer before inserting. Drug clusters then enter the lipid bilayer while the fluctuations of the acyl tails mediate the subsequent separation of the aggregate.

Umbrella simulations were conducted to generate the potential of mean force (PMF) of each carbapenem. Briefly, we generated initial trajectories by applying a harmonic potential of 1500 kJ/mol to each carbapenem along the bilayer normal, z. We then sampled every Δz = 1 Å for our initial configurations and conducted ∼50 simulation windows for 20 ns per carbapenem. The PMF profiles were generated using the GROMACS weighted histrogram analysis method (WHAM). These profiles were then averaged across leaflets and smoothed with local weighting to show the general localization of each carbappenem in the bilayer, as shown in Figure 6.

While the PMF for ertapenem, meropenem, and doripenem shows minima inside of the hydrophobic membrane core at z values of ∼10 Å (ertapenem), ∼7 Å (meropenem), and ≤5 Å (doripenem), the global minimum of imipenem is observed in the water layer, consistent with their insertion kinetics. However, the local PMF minimum at z-values of ∼5 Å indicates a potential inserted state of imipenem. This state was not observed in our MD simulations, likely because of the corresponding long time scales to populate this state against the energy barrier. The inserted state was observed in the X-ray diffraction experiments, as will be shown below. Doripenem, ertapenem, and meropenem are consistent in that there is a more stable position within the bilayer with higher instability external to the bilayer. Both doripenem and ertapenem experience a small energy minimum near the bilayer head groups, which may be attributed to the greater net dipole of these carbapenems, allowing for stable alignment with the bilayer charge gradient. These results are consistent with both bulk water simulation and experiment. We find the free energy transition from membrane to water, $\Delta G(z)_{H_2O \rightarrow MmB}$, for imipenem to be 92.6 kJ/mol, suggesting nonspontaneous insertion. Doripenem, ertapenem, and meropenem demonstrate comparable $\Delta G(z)_{H_2O \rightarrow MmB}$ at −12.8, −23.3, and −24.0 kJ/mol, respectively.

The number of drug molecules, which did not insert, can be calculated from the simulations and is shown in Figure 7a. While even at high concentrations imipenem did not partition into the bilayers within the time of the simulations of 400 ns, doripenem, ertapenem, and meropenem were found to penetrate the bilayers with time (in descending order). The number of hydrogen bonds between drug molecules and DMPC bilayers at low and high concentrations is shown in Figure 7b. While imipenem at low concentrations has the

DOI: 10.1021/acsinfecdis.7b00156
ACS Infect. Dis. 2018, 4, 926−935

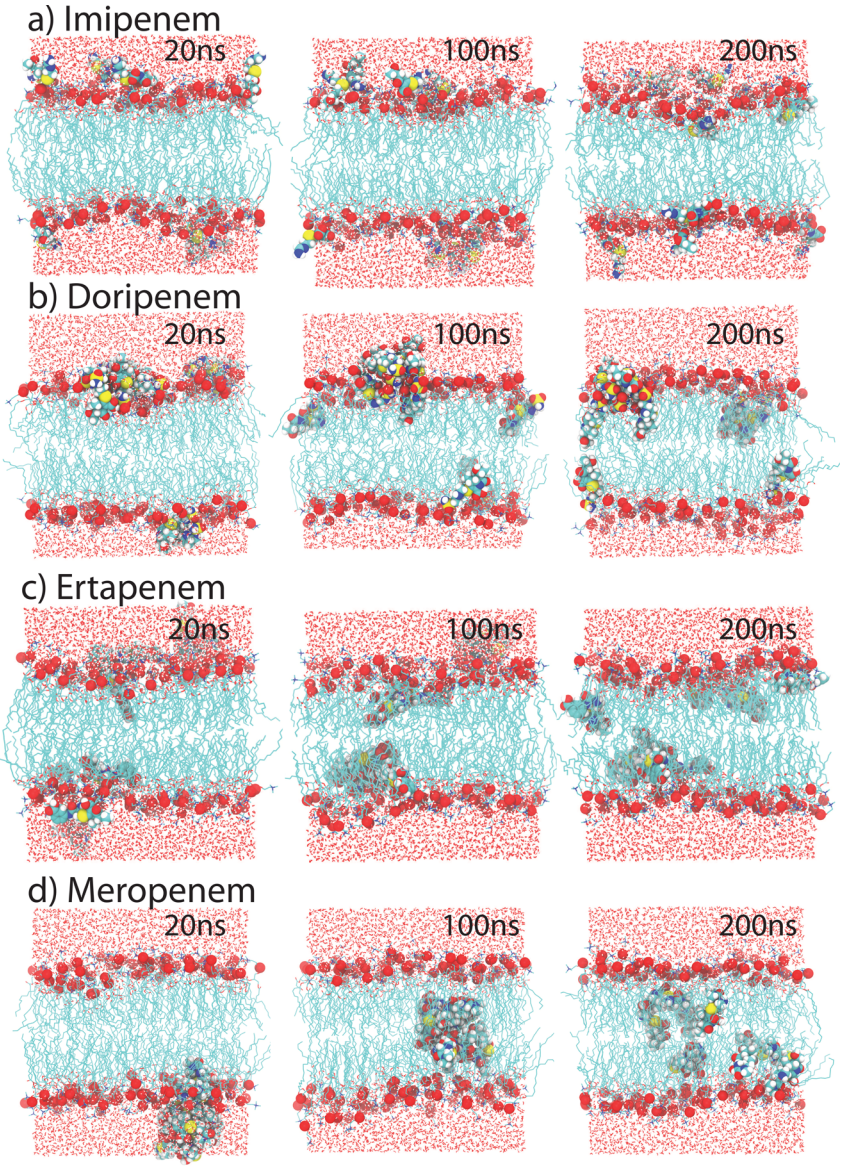

Figure 5. Snapshots of the high concentration simulations of imipenem (a), doripenem (b), ertapenem (c), and meropenem (d) at three different time windows, namely, 20, 100, and 200 ns. For doripenem, ertapenem, and meropenem, drug molecules were found to form aggregates in the aqueous phase, which then spontaneously inserted into the bilayers.

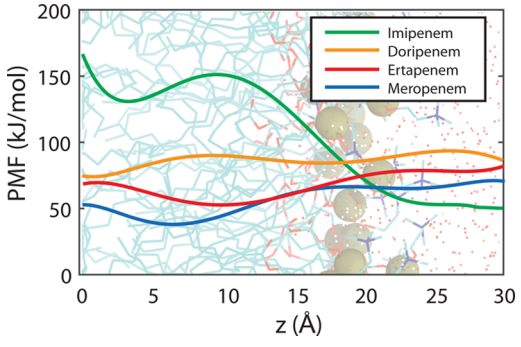

Figure 6. PMF profiles for each carbapenem at different positions in a bilayer leaflet. Umbrella windows were sampled per drug at $\Delta z = 1$ Å and averaged on the basis of the position from the bilayer center.

smallest number of bonds with the bilayers, imipenem aggregates hydrogen bind to the lipid head groups. Meropenem has the smallest number of hydrogen bonds at high concentration and completely inserts into the bilayers fast. Meropenem is interesting in that, although ten molecules were placed randomly in the water layer, the aggregate was spontaneously formed within 25 ns, and complete insertion was reached within 40 ns.

To investigate the effect of the different drugs on the bilayers, Figure 7c shows the deuterium order parameter, S, of the DMPC bilayers for the different C atoms along the lipid acyl tails. S is defined as $S = \langle(3\cos^2\theta - 1)/2\rangle$ and is a measure for the orientational mobility of the C−H bonds (θ is the angle between the C−H bond vector and the bilayer normal). A value of −0.5 ($\theta = 90°$) indicates a perfectly ordered acyl chain in all-trans conformation (rapidly rotating around the bilayer normal). Values of ∼0.20 have been reported for fluid DMPC bilayers indicating a high bond mobility.[18] The presence of the carbapenems in the bilayers led to an increase of S, related to a stiffening of the lipid tails.

X-ray diffraction of highly oriented lipid bilayers of DMPC was used to determine the position of each carbapenem in the

DOI: 10.1021/acsinfecdis.7b00156
ACS Infect. Dis. 2018, 4, 926−935

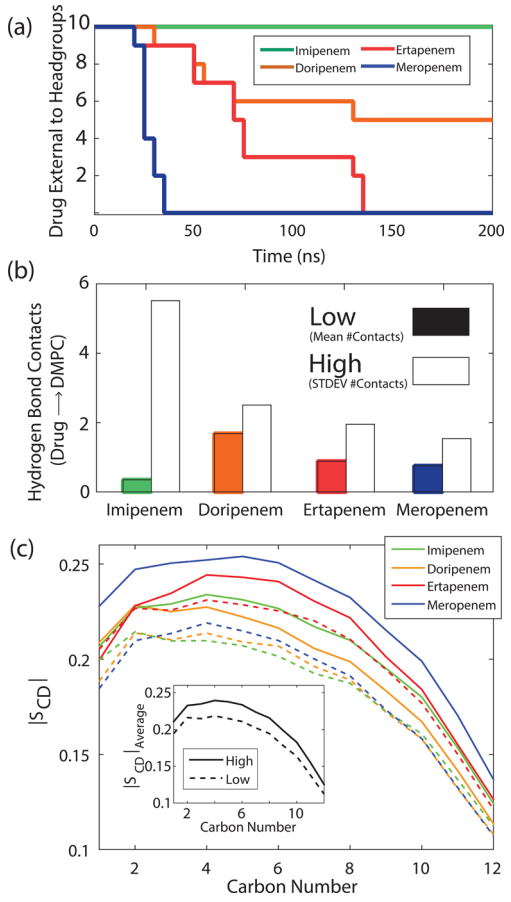

Figure 7. (a) Insertion kinetics of the drugs at high concentrations, as defined by the drug center-of-mass crossing the head−tail interface. (b) The mean number of hydrogen bonds for each drug in low concentrations (black) and the number of swapped hydrogen bonds with standard deviation of the equilibrated high concentration systems. While imipenem was found to never insert into the bilayers (within the time scales of the simulations), doripenem, ertapenem, and meropenem clusters spontaneously partitioned into the membranes. The faster the insertion kinetics, the fewer hydrogen bonds with the lipid head groups were formed. (c) The deuterium order parameters for DMPC are provided per carbon number for each tested carbapenem at high (solid) and low (dashed) concentrations. The averaged values for all tested carbapenems at high and low concentrations are shown in the subplot.

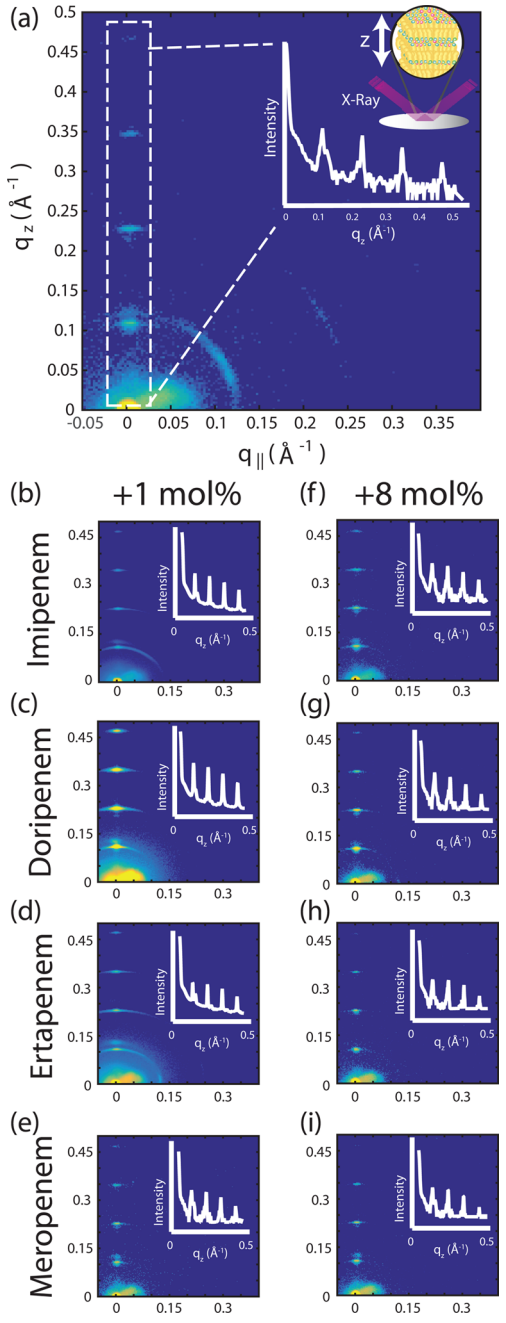

Figure 8. Two-dimensional X-ray intensity maps for all membrane assays: pure DMPC (a), DMPC + imipenem (b, f), doripenem (c, g), ertapenem (d, h), and meropenem (e, i), at low and high drug concentrations, respectively. All membrane complexes formed lamellar membranes, and lamellar Bragg peaks up to an order of 6 were used to calculate electron density profiles. Some scans show small contributions of a nonlamellar phase, likely related to lipids not part of the lamellar bilayers. On the basis of the integrated peak intensities, the volume fraction of this phase is less than about 5% in all assays. Reflectivity curves were determined by integration (as shown in part (a)), and the lamellar peak intensities were determined through fitting of peak profiles.

bilayer. Briefly, lipid membranes of DMPC were prepared with identical molar concentrations as in the simulations. Bilayers were scanned inside of a hydration chamber at a relative humidity (RH) of 97% and at a temperature of 28 °C, in the physiologically relevant fluid phase of the bilayers. Reflectivity profiles for all membrane complexes are shown in Figure 8. All bilayers formed well oriented lamellar membranes, and lamellar Bragg peaks up to an order of 6 were observed. Integrated peak intensities were used for the calculation of electron density profiles, as described in the Methods section.

The electron densities, $\rho(z)$, of pure DMPC and DMPC + 1 mol % of the drug and + 10 mol % of the drug are shown in Figure 9a−d. The location of the molecules can be determined from the difference curves between the 1 mol % and pure DMPC bilayer, $\Delta\rho(z)$, also shown in Figure 9. We observe imipenem to be mainly localized in the headgroup at 17.3 Å. A second, smaller population is observed at z-values of about 7 Å, in agreement with the PMF calculations. The remaining carbapenems localized in the tail groups with meropenem at 10 Å, doripenem at 8.2 Å, and ertapenem at 7.6 Å (measured from the center of the bilayer). Electron density profiles calculated from the MD simulations are shown in Figure 9e−h. In simulations, it is straightforward to determine the position of

DOI: 10.1021/acsinfecdis.7b00156
ACS Infect. Dis. 2018, 4, 926−935

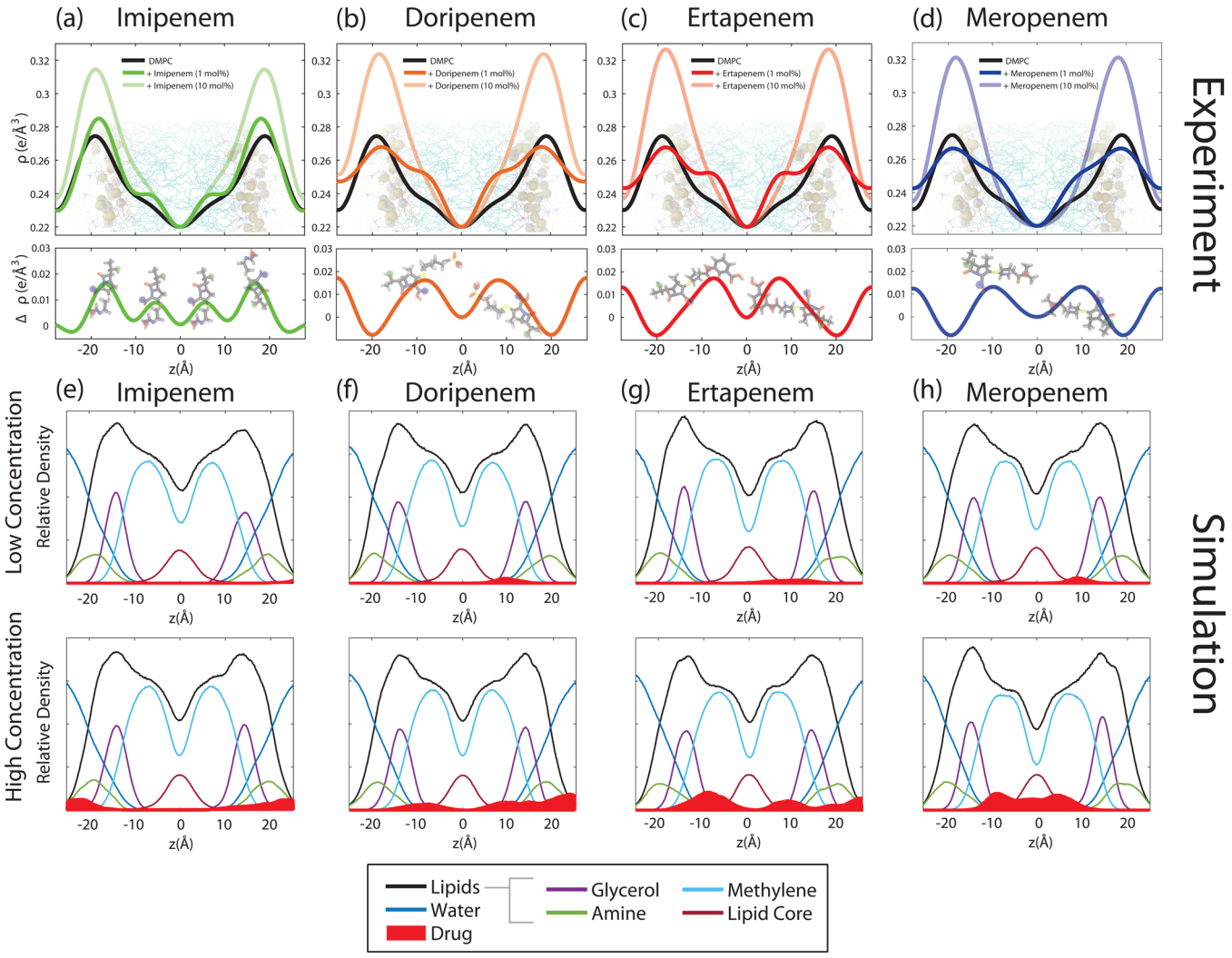

Figure 9. Experimentally determined electron density profiles for imipenem (a), doripenem (b), ertapenem (c), and meropenem (d). The difference profiles between low concentrations of carbapenems and pure bilayers can be assigned to the drug molecules, and the positions of the different carbapenems are shown. (e–h) The electron densities for low and high drug concentrations, as calculated from the MD simulations. Position of the molecules from experimentally and theoretically calculated electron densities and PMF calculations show an excellent agreement. Drug molecules are drawn at their respective position, in agreement with the tilt angles found in the MD simulations in Figure 4.

lipids and water and drug molecules. The position of the glycerol, amine, methylene groups, and the lipid core were also calculated. The positions of the different drug molecules are in excellent agreement with the experimentally determined positions and the PMF calculations. We note that the inserted state of imipenem was not observed in the simulations within the 400 ns of simulations.

DISCUSSION

The interaction of imipinem, doripenem, ertapenem, and meropenem with lipid membranes was investigated from MD simulations and X-ray diffraction experiments. At low drug concentrations, all drugs except imipenem partition into the lipid tail groups within ∼40 ns; however, the insertion dynamics of each drug differ significantly. Both doripenem and ertapenem molecules rotate as they cross the head–tail interface, maintaining the hydrogen bonding between the amine group and the lipid head groups. The conservation of this bond leads to a coarse severation of the lipid heads laterally as the drugs insert. Meropenem obeys a more conservative insertion in which the drug shows minimal rotation while sliding between lipids causing minimal headgroup severation. Imipenem showed no insertion over 400 ns of simulation at either concentration.

From PMF profiles and experimentally determined electron density profiles, we observe the most stable position of imipenem in the lipid head groups, while doripenem, meropenem, and ertapenem are stabilized in the hydrophobic acyl tails. As the head-core membrane spacing of a pure DMPC bilayer is found to be 19.2 Å at 97% RH conditions, we find imipenem to intercalate and localize at a distance of 17.3 Å from the core. PMF and experiments also indicate an inserted state of imipenem at ∼7 Å, separated by an energy barrier. This state was not observed within the 400 ns of MD simulations, likely because of the corresponding long time scales. The highly membrane soluble carbapenems are positioned within ⩽10 Å of the membrane core, organizing completely within the acyl tails. From the deuterium order parameter, the presence of carbapenems increases bilayer rigidity.

At high concentrations of carbapenems, the drugs were found to create aggregates in the aqueous layer. Computing the radial distribution functions (RDFs) of the drugs with respect

DOI: 10.1021/acsinfecdis.7b00156
ACS Infect. Dis. 2018, 4, 926–935

to one another showed no functional organization within the bilayer. Rather, the drug molecules form aggregates within the water layer which collectively adsorb into the bilayer, drawing a large volume of water into the membranes.

While carbapenems have enzyme targets and can be transported into the periplasm without membrane contact,[19] specifically transpeptidases, the physical interactions between carbapenems and the lipid bilayer present at the interfaces of the bacterial periplasm may play a significant role in previous observations. For example, carbapenemases, which inactivate carbapenems, are water-soluble and have a 10-fold greater specificity for imipenem relative to meropenem.[20] This may be due to the partial partitioning of meropenem in the bilayer, protecting the active β-lactam group from hydrolysis.

After the carbapenem is translocated to the periplasm, the molecule's binding site in DD-transpeptidase may be stabilized by the membrane. However, carbapenem motion is not random in this phase, and for this reason, the motion of the drug molecules can be driven toward the membranes increasing their association constant with the DD-transpeptidase. Imipenem's increased MIC in many Gram-negative bacterial strains, as shown in Figure 10, may be due to its greater stability in this

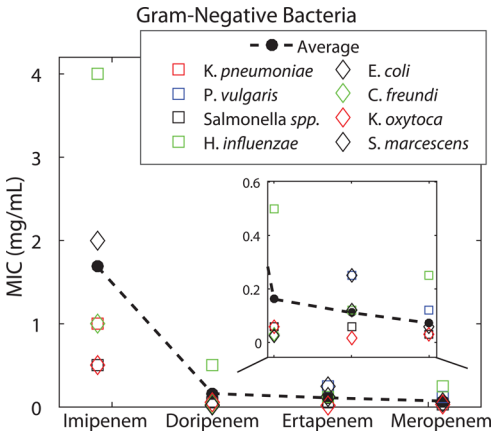

Figure 10. MIC values for Gram-negative bacteria from Zhanel et al.[4] Imipenem's increased MIC in many Gram-negative bacterial strains may be related to its greater stability in the aqueous phase.

aqueous phase, whereas the association of the larger carbapenems, doripenem, ertapenem, and meropenem, is enhanced by slight affinity for the membrane acyl tails. Membrane partitioning may, thus, be relevant for effective drug design in order to maximize association with the target enzyme for carbapenems.

CONCLUSION

MD simulations and X-ray diffraction experiments of imipenem, meropenem, doripenem, and ertapenem were used to investigate their interaction with lipid bilayers. While imipenem did not partition in the lipid membranes during 400 ns of MD simulations, all other drugs spontaneously inserted into the membranes. Membrane solubility was found to decrease from imipenem to doripenem, ertapenem, and finally meropenem. At low concentrations, membrane insertion was found to be a two step process, where the drugs first adsorb to the lipid head groups and finally insert through a rotation of the molecule. At higher drug concentrations, the molecules were found to form aggregates in the aqueous phase before making contact with the membranes and spontaneously inserting into the bilayers, best described by a three step process. The presence of the drugs led to an increase of the deuterium order parameter, indicative of a membrane stiffening.

Positions of the drugs were determined from experiments and simulations. Imipenem was found to be mainly localized in the headgroup at ~17 Å. A second, inserted population was observed at z-values of about 7 Å in experiments and in calculations of the potential of mean force (PMF). This population was not observed in the MD simulations, likely due to the long time scales involved. The remaining carbapenems were found to localize in the tail groups with meropenem at ~10 Å, doripenem at ~8 Å, and ertapenem at ~8 Å (measured from the center of the bilayer). Drug efficacy is likely also related to membrane absorption, which can enhance the availability of the drug to the target penicillin-binding proteins, where their targets are located. The results show that membrane interactions of drugs can play an important role for the clinical efficacy and should be considered in drug design.

METHODS

Molecular Dynamics Simulations. A system of 128 DMPC lipids (64 per leaflet) was taken from Tieleman et al.[21] and independently equilibrated for 500 ns. Drug topologies were constructed using the Automated Topology Builder (ATB), computing partial charges using quantum mechanical optimization at the B3LYP/6-31G* level of theory.[22,23] The SPC water model was used for system solvation.[24] All MD simulations were performed using the GROMACS 5.1.4 software package,[25] implementing the GROMOS 54a7 force field[26] modified with Berger lipid parameters.[27] Hydrogen atoms in the acyl tails are considered to be part of the carbon sequence in this (united atom) model and Mulliken partial charges were calculated using Antechamber. All other components were simulated with all atom-topologies. All simulations used a 2 fs time step; periodic boundary conditions were applied in all directions, and the particle-mesh Ewald (PME) was used to solve for long-range electrostatics.[28] A short-range van der Waals cutoff of 1.2 nm and a short-range electrostatic cutoff of 1.0 nm were used. The P-LINCS algorithm was used to determine bond constraints.[29] A Fourier spacing of 0.16 nm was used with cubic interpolation. The Verlet group scheme was used for group pair lists, which were updated every 10 fs. Temperature coupling was controlled using a Nose-Hoover thermostat at 27 °C (τ = 0.5 ps),[30,31] and semi-isotropic coupling was used to maintain a pressure at 1.0 bar using a Parrinello−Rahman barostat (τ = 1 ps).[32] An overview of all systems prepared for the MD simulations is shown in Table 1.

Simulations containing pure DMPC at low (one molecule) and high (ten molecules) concentrations of the carbapenems ran at 30 water molecules per lipid for 200 ns each (400 ns for imipenem). For the systems containing carbapenems, the solute molecules were placed within the aqueous water layer randomly using a Monte Carlo method. All analyses were performed with the final 10 ns of the simulations (unless stated otherwise) using GROMACS algorithms and simple scripts.[33] Deuterium order was calculated for the acyl chains in the lipid patch using the built-in gmx order script. This is a measure of the lipid ordering, and a surrogate measure for lipid rigidity, and is often used to rationalize the effects of peptides on lipid bilayers.[34]

Umbrella Simulations. Umbrella simulations were performed, with the protocol based on previous studies. Initially, a single carbapenem molecule was placed at the edge of the

DOI: 10.1021/acsinfecdis.7b00156
ACS Infect. Dis. 2018, 4, 926−935

Table 1. Summary of Simulated Systems[a]

system	# molecules	runtime (ns)
DMPC		500
+imipenem	1	400
+imipenem	10	200
+doripenem	1	200
+doripenem	10	200
+ertapenem	1	200
+ertapenem	10	200
+meropenem	1	200
+meropenem	10	200

[a]Listed are the composition, number of drug molecules, simulation runtime.

system box, and a force constant of 1500 kJ/mol was applied to the molecule in the z direction. Umbrella windows were obtained with Δz = 1 Å, and each window was simulated for 20 ns. Potential of mean forces (PMFs) were then calculated using the weighted histogram analysis method in GROMACS, with the final 5 ns of each umbrella window with the center of the bilayer as the reference point.

X-ray Diffraction. Highly oriented multilamellar membranes were prepared on single-side polished silicon wafers. 1,2-Dimyristoyl-*sn*-glycero-3-phosphocholine (DMPC, Avanti Polar Lipids) was mixed with imipenem, ertapenem, meropenem (Abcam), or doripenem (Sigma) at low (1 mol %) or high (10 mol %) concentrations in a 2,2,2-trifluoroethanol/chloroform (1:1, vol/vol) mixture at a solution concentration of 18 mg/mL. Wafers were sonicated in 1,2-dichloromethane for 30 min and then rinsed with alternating methanol and 18.2 MΩ cm water. The wafers were dried using nitrogen, and 75 μL of solution was deposited. After drying, the samples were placed in a vacuum for 24 h at 310 K to remove solvent and incubated at T = 50 °C and RH = 97% for 3 days to anneal membrane structure.

Out-of-plane X-ray scattering data was obtained using the Biological Large Angle Diffraction Experiment (BLADE) at McMaster University. BLADE uses a 9 kW (45 kV, 200 mA) Cu Kα rotating anode at a wavelength of 1.5418 Å. Both source and detector are mounted on moveable arms such that the membranes stay horizontal during measurements. Focusing, multilayer optics provide a high intensity collimated, 200 μm sized beam with monochromatic X-ray intensities up to 10^8 counts/s. Scattering was detected using a Rigaku HyPix-3000 2D semiconductor detector with an area of 3000 mm^2 and 100 μm pixel size.

Electron density profiles were determined from specular reflectivity. The relative electron density, $\rho(z)$, is approximated by a 1-dimensional Fourier analysis,

$$\rho(z) = \frac{2}{d_z}\sum_{n=1}^{N}\sqrt{I_n q_n}\,\nu_n \cos\left(\frac{2\pi n z}{d_z}\right) \quad (1)$$

N is the highest order of the Bragg peaks observed in the experiment. The integrated peak intensities, I_n, are multiplied by q_n to receive the form factors, $F(q_n)$.[35,36] The bilayer form factor $F(q_z)$, which is in general a complex quantity, is real-valued in the case of centro-symmetry. The phase problem of crystallography, therefore, simplifies to the sign problem $F(q_z) = \pm|F(q_z)|$ and the phases, ν_n, can only take the values ±1. The phases ν_n are needed to reconstruct the electron density profile from the scattering data following eq 1 and are well-defined for DMPC at 97% RH from our previous work.[37]

$\rho(z)$ is initially calculated on an arbitrary scale; they are then scaled on the basis of the protocol established in our previous work.[37] The curves are scaled until the total number of electrons within the lipid unit cell across a membrane leaflet, $e^- = A_L\int_0^{d_z/2}\rho(z)\,dz$, agrees with the total number of electrons expected on the basis of the sample composition. An area per lipid (A_L) of 60 Å for a hydrated DMPC bilayer at 27 °C was used, as reported in ref 38.

AUTHOR INFORMATION

Corresponding Author

*E-mail: rheinstadter@mcmaster.ca. Phone: +1-(905)-525-9140-23134. Fax: +1-(905)-546-1252.

ORCID

Maikel C. Rheinstädter: 0000-0002-0558-7475

Author Contributions

A.K. prepared membrane samples, conducted X-ray experiments, analyzed X-ray data, conducted MD simulations, analyzed MD data, and wrote the manuscript. A.K.D. conducted MD simulations and analyzed MD data. D.J.M. conducted MD simulations and analyzed MD data. M.C.R. conceived of the study, designed the study, coordinated the study, analyzed data, and wrote the manuscript. All authors gave final approval for publication.

Notes

The authors declare no competing financial interest.

ACKNOWLEDGMENTS

This research was funded by the Natural Sciences and Engineering Research Council of Canada (NSERC), the Canada Foundation for Innovation (CFI), the Canadian Institute of Health Research (CIHR), and the Ontario Ministry of Economic Development and Innovation. A.K. is a recipient of a CIHR Undergraduate Studentship (Grant No. 153486). D.J.M. is the recipient of an OGF Award. A.K.D. is the recipient of an NSERC USRA, and M.C.R. is the recipient of an Early Researcher Award of the Province of Ontario and a University Scholar Award from McMaster University.

ABBREVIATIONS

MD, molecular dynamics; DMPC, 1,2-dimyristoyl-*sn*-glycero-3-phosphocholine; MIC, minimum inhibitory concentration; PMF, potential of mean force; RDF, radial distribution function

REFERENCES

(1) Brown, E. D., and Wright, G. D. (2016) Antibacterial drug discovery in the resistance era. *Nature 529*, 336−343.

(2) Nikaido, H. (2009) Multidrug resistance in bacteria. *Annu. Rev. Biochem. 78*, 119−146.

(3) Papp-Wallace, K. M., Endimiani, A., Taracila, M. A., and Bonomo, R. A. (2011) Carbapenems: past, present, and future. *Antimicrob. Agents Chemother. 55*, 4943−4960.

(4) Zhanel, G. G., Wiebe, R., Dilay, L., Thomson, K., Rubinstein, E., Hoban, D. J., Noreddin, A. M., and Karlowsky, J. A. (2007) Comparative review of the carbapenems. *Drugs 67*, 1027−1052.

(5) Masuda, N., Sakagawa, E., and Ohya, S. (1995) Outer membrane proteins responsible for multiple drug resistance in Pseudomonas aeruginosa. *Antimicrob. Agents Chemother. 39*, 645−649.

(6) Zapun, A., Macheboeuf, P., and Vernet, T. (2017) *Antimicrobial Drug Resistance*, pp 177−211, Springer, New York.

DOI: 10.1021/acsinfecdis.7b00156
ACS Infect. Dis. 2018, 4, 926−935

(7) Van Oosten, B., Marquardt, D., and Harroun, T. A. (2017) Testing High Concentrations of Membrane Active Antibiotic Chlorhexidine Via Computational Titration and Calorimetry. *J. Phys. Chem. B 121*, 4657−4668.
(8) Ogawa, K., Yumoto, R., Hamada, N., Nagai, J., and Takano, M. (2006) Interaction of valproic acid and carbapenem antibiotics with multidrug resistance-associated proteins in rat erythrocyte membranes. *Epilepsy Res. 71*, 76−87.
(9) Livermore, D. M. (2001) Of Pseudomonas, porins, pumps and carbapenems. *J. Antimicrob. Chemother. 47*, 247−250.
(10) Brogden, K. A. (2005) Antimicrobial peptides: pore formers or metabolic inhibitors in bacteria? *Nat. Rev. Microbiol. 3*, 238.
(11) Silva, J. R. A., Roitberg, A. E., and Alves, C. N. (2014) Catalytic mechanism of L, D-transpeptidase 2 from Mycobacterium tuberculosis described by a computational approach: insights for the design of new antibiotics drugs. *J. Chem. Inf. Model. 54*, 2402−2410.
(12) Park, H., and Merz, K. M. (2005) Force field design and molecular dynamics simulations of the carbapenem-and cephamycin-resistant dinuclear zinc metallo-β-lactamase from Bacteroides fragilis and its complex with a biphenyl tetrazole inhibitor. *J. Med. Chem. 48*, 1630−1637.
(13) John, T., Thomas, T., Abel, B., Wood, B. R., Chalmers, D. K., and Martin, L. L. (2017) How kanamycin a interacts with bacterial and mammalian mimetic membranes. *Biochim. Biophys. Acta, Biomembr. 1859*, 2242.
(14) Giannoni, E., Moreillon, P., Cotting, J., Moessinger, A., Bille, J., Décosterd, L., Zanetti, G., Majcherczyk, P., and Bugnon, D. (2006) Prospective determination of plasma imipenem concentrations in critically ill children. *Antimicrob. Agents Chemother. 50*, 2563−2568.
(15) Esterly, J. S., Wagner, J., McLaughlin, M. M., Postelnick, M. J., Qi, C., and Scheetz, M. H. (2012) Evaluation of clinical outcomes in patients with bloodstream infections due to Gram-negative bacteria according to carbapenem MIC stratification. *Antimicrob. Agents Chemother. 56*, 4885−4890.
(16) Neidhardt, F. C., Ingraham, J. L., and Schaechter, M. (1990) *Physiology of the bacterial cell: a molecular approach*, Vol. *20*, Sinauer, Sunderland.
(17) Khondker, A., Dhaliwal, A., Alsop, R. J., Tang, J., Backholm, M., Shi, A.-C., and Rheinstädter, M. C. (2017) Partitioning of caffeine in lipid bilayers reduces membrane fluidity and increases membrane thickness. *Phys. Chem. Chem. Phys. 19*, 7101−7111.
(18) Vermeer, L. S., De Groot, B. L., Réat, V., Milon, A., and Czaplicki, J. (2007) Acyl chain order parameter profiles in phospholipid bilayers: computation from molecular dynamics simulations and comparison with 2 H NMR experiments. *Eur. Biophys. J. 36*, 919−931.
(19) Kojima, S., and Nikaido, H. (2013) Permeation rates of penicillins indicate that Escherichia coli porins function principally as nonspecific channels. *Proc. Natl. Acad. Sci. U. S. A. 110*, E2629−E2634.
(20) Queenan, A. M., and Bush, K. (2007) Carbapenemases: the versatile β-lactamases. *Clin. Microbiol. Rev. 20*, 440−458.
(21) Tieleman, D. P., Sansom, M. S., and Berendsen, H. J. (1999) Alamethicin helices in a bilayer and in solution: molecular dynamics simulations. *Biophys. J. 76*, 40−49.
(22) Malde, A. K., Zuo, L., Breeze, M., Stroet, M., Poger, D., Nair, P. C., Oostenbrink, C., and Mark, A. E. (2011) An automated force field topology builder (ATB) and repository: version 1.0. *J. Chem. Theory Comput. 7*, 4026−4037.
(23) Koziara, K. B., Stroet, M., Malde, A. K., and Mark, A. E. (2014) Testing and validation of the Automated Topology Builder (ATB) version 2.0: prediction of hydration free enthalpies. *J. Comput.-Aided Mol. Des. 28*, 221−233.
(24) Berendsen, H. J., Postma, J. P., van Gunsteren, W. F., and Hermans, J. (1981) *Intermolecular Forces*, pp 331−342, Springer, New York.
(25) Abraham, M. J., Murtola, T., Schulz, R., Páll, S., Smith, J. C., Hess, B., and Lindahl, E. (2015) GROMACS: High performance molecular simulations through multi-level parallelism from laptops to supercomputers. *SoftwareX 1-2*, 19−25.
(26) Schmid, N., Eichenberger, A. P., Choutko, A., Riniker, S., Winger, M., Mark, A. E., and van Gunsteren, W. F. (2011) Definition and testing of the GROMOS force-field versions 54A7 and 54B7. *Eur. Biophys. J. 40*, 843−856.
(27) Berger, O., Edholm, O., and Jähnig, F. (1997) Molecular dynamics simulations of a fluid bilayer of dipalmitoylphosphatidylcholine at full hydration, constant pressure, and constant temperature. *Biophys. J. 72*, 2002.
(28) Darden, T., York, D., and Pedersen, L. (1993) Particle mesh Ewald: An N log (N) method for Ewald sums in large systems. *J. Chem. Phys. 98*, 10089−10092.
(29) Hess, B., Bekker, H., Berendsen, H. J., and Fraaije, J. G. (1997) LINCS: a linear constraint solver for molecular simulations. *J. Comput. Chem. 18*, 1463−1472.
(30) Nosé, S. (1984) A unified formulation of the constant temperature molecular dynamics methods. *J. Chem. Phys. 81*, 511−519.
(31) Hoover, W. G. (1985) Canonical dynamics: equilibrium phase-space distributions. *Phys. Rev. A: At., Mol., Opt. Phys. 31*, 1695.
(32) Parrinello, M., and Rahman, A. (1981) Polymorphic transitions in single crystals: A new molecular dynamics method. *J. Appl. Phys. 52*, 7182−7190.
(33) Van Der Spoel, D., Lindahl, E., Hess, B., Groenhof, G., Mark, A. E., and Berendsen, H. J. (2005) GROMACS: fast, flexible, and free. *J. Comput. Chem. 26*, 1701−1718.
(34) Gapsys, V., de Groot, B. L., and Briones, R. (2013) Computational analysis of local membrane properties. *J. Comput.-Aided Mol. Des. 27*, 845−858.
(35) Nagle, J. F., and Wiener, M. C. (1989) Relations for lipid bilayers. Connection of electron density profiles to other structural quantities. *Biophys. J. 55*, 309.
(36) Barrett, M. A., Zheng, S., Roshankar, G., Alsop, R. J., Belanger, R., Huynh, C., Kučerka, N., and Rheinstädter, M. C. (2012) Interaction of aspirin (acetylsalicylic acid) with lipid membranes. *PLoS One 7*, e34357.
(37) Alsop, R. J., Khondker, A., Hub, J. S., and Rheinstädter, M. C. (2016) The Lipid Bilayer Provides a Site for Cortisone Crystallization at High Cortisone Concentrations. *Sci. Rep. 6*, 22425.
(38) Kučerka, N., Nieh, M.-P., and Katsaras, J. (2011) Fluid phase lipid areas and bilayer thicknesses of commonly used phosphatidylcholines as a function of temperature. *Biochim. Biophys. Acta, Biomembr. 1808*, 2761−2771.

DOI: 10.1021/acsinfecdis.7b00156
ACS Infect. Dis. 2018, 4, 926−935